

## RESEARCH ARTICLE

View Article Online

View Journal | View Issue

Cite this: *Inorg. Chem. Front.*, 2025, **12**, 138

## A novel cerium-based metal–organic framework supported Pd catalyst for semi-hydrogenation of phenylacetylene†

Xiangdi Zeng,<sup>a</sup> Zi Wang,<sup>a</sup> Meng He,<sup>a</sup> Wanpeng Lu,<sup>a</sup> Wenyuan Huang,<sup>b</sup> Bing An,<sup>a</sup> Jiangnan Li,<sup>b</sup> Mufan Li,<sup>b</sup> Ben F. Spencer,<sup>c</sup> Sarah J. Day,<sup>d</sup> Floriana Tuna,<sup>a,e</sup> Eric J. L. McInnes,<sup>a</sup> Martin Schröder<sup>a</sup> and Sihai Yang<sup>a,b</sup>

Phenylacetylene is a detrimental impurity in the polymerisation of styrene, capable of poisoning catalysts even at ppm levels and significantly degrading the quality of polystyrene. The semi-hydrogenation of phenylacetylene to styrene instead of ethylbenzene is, therefore, an important industrial process. We report a novel cerium(IV)-based metal–organic framework (denoted as Ce-bptc), which comprises {Ce<sub>6</sub>} clusters bridged by biphenyl-3,3',5,5'-tetracarboxylate linkers. Ce-bptc serves as an ideal support for palladium nanoparticles and the Pd@Ce-bptc catalyst demonstrates excellent catalytic performance for semi-hydrogenation of phenylacetylene, achieving a selectivity of 93% towards styrene on full conversion under ambient conditions with excellent reusability. *In situ* synchrotron X-ray powder diffraction and electron paramagnetic resonance spectroscopy reveal the binding domains of phenylacetylene within Ce-bptc, and details of the reaction mechanism are discussed.

Received 2nd September 2024,

Accepted 30th October 2024

DOI: 10.1039/d4qi02225d

rsc.li/frontiers-inorganic

## Introduction

Phenylacetylene is a key impurity that harms the polymerisation of styrene; even concentrations of just a few dozen ppm can poison the catalyst and significantly degrade the quality of polystyrene.<sup>1</sup> Therefore, semi-hydrogenation of phenylacetylene to styrene, rather than the undesired ethylbenzene, is of great importance to the polystyrene industry.<sup>2</sup> Palladium metal nanoparticles are the leading catalysts for this reaction.<sup>3,4</sup> To maximise the utilisation of noble metals and stabilise Pd nanoparticles, doping them into porous materials, such as zeolites, carbons and metal–organic frameworks (MOFs), has been investigated.<sup>5–11</sup> In this context, the porous supports have notable impacts on the catalytic activity of Pd

nanoparticles, and MOFs have received much attention due to their high structural diversity and tuneability.<sup>5</sup> For example, Pd nanoparticles supported on the UiO-series of MOFs have shown an exceptional TOF (turnover frequency) of 13 835 h<sup>−1</sup>.<sup>9</sup> The hydrophobicity of the ligand in the porous material can also influence the catalytic activity of the supported Pd nanoparticles. It has been reported that functional groups on the pore surface can promote charge transfer between the porous support and Pd sites, giving rise to an improved catalytic performance.<sup>9,11</sup> Additionally, the metal centres in MOFs can also influence the catalytic microenvironment. Compared with Zr-based MOFs,<sup>9</sup> Ce-based MOFs often contain both Ce(III) and Ce(IV) sites, which can act as an internal redox couple. Thus, Ce-MOFs can promote charge transfer to facilitate various redox reactions<sup>12–14</sup> and, we argued, may function as excellent catalyst supports for semi-hydrogenation reactions.

Herein, we report a novel Ce(IV)-based MOF (Ce-bptc), consisting of {Ce<sub>6</sub>} clusters bridged by biphenyl-3,3',5,5'-tetracarboxylate linkers. Incorporation of Pd nanoparticles onto Ce-bptc affords an efficient catalyst Pd@Ce-bptc for the semi-hydrogenation of phenylacetylene, yielding a selectivity of 93% towards styrene on full conversion under ambient conditions. The catalytic mechanism has been elucidated by *in situ* synchrotron X-ray powder diffraction (SXPD), X-ray photoelectron spectroscopy (XPS), and electron paramagnetic resonance (EPR) spectroscopy.

<sup>a</sup>Department of Chemistry, University of Manchester, Manchester, M13 9PL, UK.  
E-mail: M.Schroder@manchester.ac.uk

<sup>b</sup>College of Chemistry and Molecular Engineering, Beijing National Laboratory for Molecular Sciences, Peking University, Beijing, 100871, China.  
E-mail: Sihai.Yang@pku.edu.cn

<sup>c</sup>Department of Materials, The University of Manchester, Manchester, M13 9PL, UK

<sup>d</sup>Diamond Light Source, Harwell Science Campus, Didcot, Oxfordshire, OX11 0DE, UK

<sup>e</sup>Photon Science Institute, University of Manchester, Manchester, M13 9PL, UK

†Electronic supplementary information (ESI) available. CCDC 2205374 and 2205379. For ESI and crystallographic data in CIF or other electronic format see DOI: <https://doi.org/10.1039/d4qi02225d>



## Results and discussion

A microcrystalline sample of Ce-bptc was synthesised by solvothermal reaction of  $(\text{NH}_4)_2\text{Ce}(\text{NO}_3)_6$  and biphenyl-3,3',5,5'-tetracarboxylic acid ( $\text{H}_4\text{bptc}$ ). Rietveld refinement of high resolution SXP data for Ce-bptc,  $\{\text{Ce}_6\text{O}_4(\text{OH})_4(\text{bptc})_3 \cdot (\text{H}_3\text{O})_{1.6} \cdot 3\text{DMF} \cdot 10\text{H}_2\text{O}\}$ , revealed that the crystal structure comprises of twelve connected  $\{\text{Ce}_6\text{O}_4(\text{OH})_4(\text{CO}_2)_{12}\}$  clusters, which are bridged by tetracarboxylate ligands to form an open and neutral framework of *ftw* topology<sup>15,16</sup> (Fig. 1a and Table S1†).

In Ce-bptc six Ce(IV) centers are assembled into an octahedron, where the eight faces are occupied by  $\mu_3\text{-O}^{2-}$  or  $\mu_3\text{-OH}^-$  groups in each  $\{\text{Ce}_6\text{O}_4(\text{OH})_4(\text{CO}_2)_{12}\}$  cluster. The Ce(IV) atom is coordinated to eight O atoms, four of which belong to four different bptc<sup>4-</sup> ligands and the remaining four are from  $\mu_3\text{-O}^{2-}/\text{OH}^-$  groups. Each bptc<sup>4-</sup> ligand is connected to four different  $\{\text{Ce}_6\}$  clusters with each carboxylate coordinated by two adjacent Ce(IV) centers in the same cluster. Ce-bptc shows cubic cages with  $\{\text{Ce}_6\}$  clusters on the vertices and a planar bptc<sup>4-</sup> linker on the faces (Fig. 1b). The cubic cages have a dimension of  $\sim 9.4$  Å and are interconnected through smaller tetrahedral cages (dimension of  $\sim 3.5$  Å) located at the twelve edges of the cubic cages (Fig. 1c). Thermogravimetric analysis (TGA) shows that Ce-bptc is stable up to *ca.* 250 °C before decomposition (Fig. S10†).

To encapsulate Pd nanoparticles, Pd precursors (at 0.3, 2.0, 3.7 and 5.4 wt%) were dissolved in water and then embedded within Ce-bptc using a double solvent method<sup>17</sup>. This was followed by treatment under a flow of  $\text{H}_2$  at 150 °C for 2 h to

yield Pd@Ce-bptc, which shows retention of the framework structure of Ce-bptc as confirmed by powder X-ray diffraction (PXRD, Fig. 2a and S1†). No obvious Bragg peaks for Pd nanoparticles or  $\text{PdO}_x$  were observed, indicating the excellent dispersion of Pd species in Ce-bptc. The diffuse reflectance infrared Fourier transform spectra (DRIFTS) of Ce-bptc and Pd@Ce-bptc confirm the retention of the structure and stretching mode of  $\mu_3\text{-OH}^-$  groups upon Pd doping (Fig. 2b). The encaps-

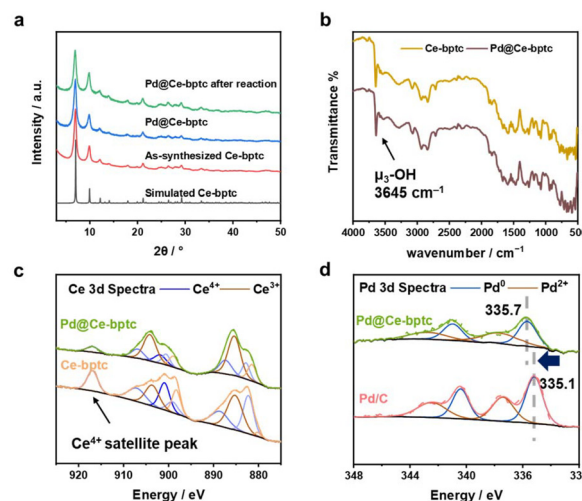


**Fig. 2** (a) PXRD patterns for Ce-bptc (as-synthesized and simulated) and for Pd@Ce-bptc before and after reaction. (b) DRIFT spectra of Ce-bptc and Pd@Ce-bptc. (c) XPS Ce 3d spectra of Ce-bptc and Pd@Ce-bptc. (d) XPS Pd 3d spectra of Pd@Ce-bptc and Pd/C.

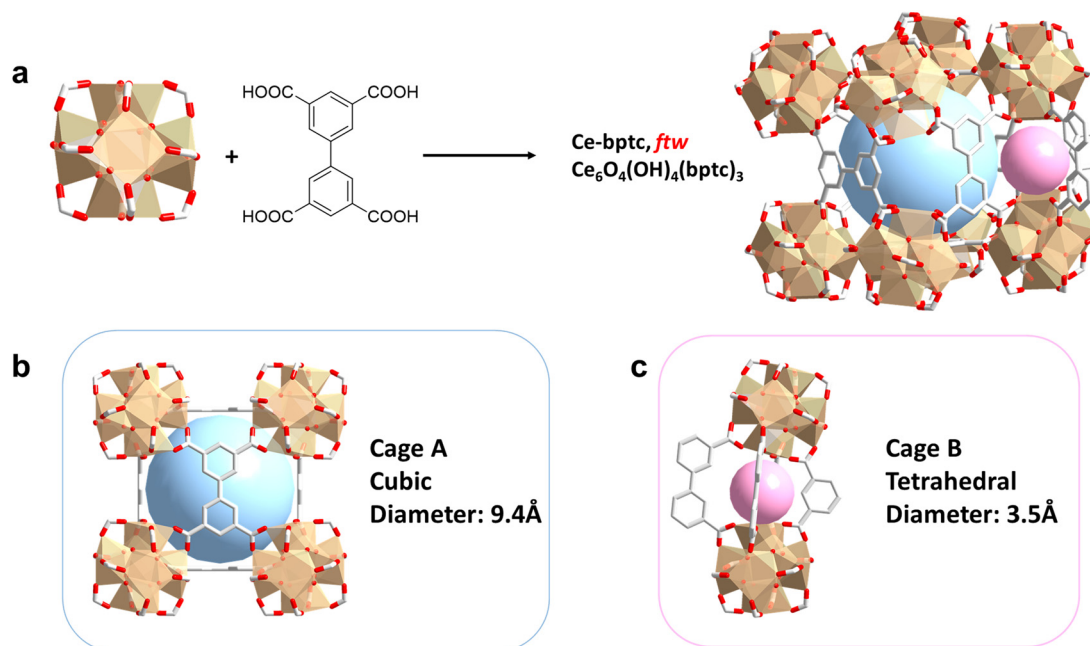


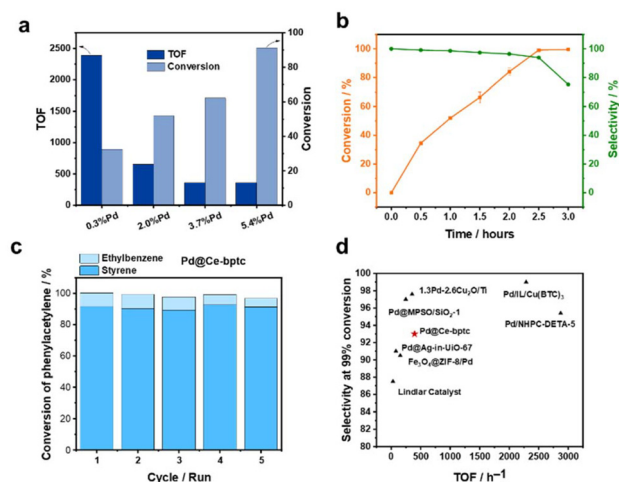
**Fig. 1** Crystal structure of Ce-bptc. (a) Views of the  $\{\text{Ce}_6\}$  cluster, linker and caged structure of Ce-bptc. (b) Detailed view of cage A (cubic cage). (c) Detailed view of cage B (tetrahedral cage). Colour code: Ce, light brown; C, grey; O, red; H, omitted for clarity. Cage A and Cage B are highlighted by blue and pink spheres, respectively.

sulation of Pd nanoparticles in Ce-bptc is also accompanied by a reduction of the Brunauer–Emmett–Teller (BET) surface area from 532 to 390 m<sup>2</sup> g<sup>−1</sup> for Ce-bptc and Pd@Ce-bptc, respectively (Fig. S3†). Scanning electron microscopy (SEM) and energy dispersive X-ray (EDX) analysis show that Pd nanoparticles are distributed homogeneously in the MOF (Fig. S7 and S8). For comparison, we also prepared another benchmark MOF, Ce-Uio-66,<sup>12</sup> which shows reduced crystallinity and almost no porosity upon the encapsulation of Pd (Fig. S2 and S9†).

XPS experiments were conducted to study the electronic state of Ce and Pd sites (Fig. 2c and d). The Ce 3d spectra were analysed according to well-established models;<sup>18</sup> it was found that both Ce(IV) and Ce(III) species (73.4% and 26.6%, respectively) exist in Ce-bptc, which is consistent with other reported Ce(IV)-based MOFs.<sup>19</sup> Upon reduction, the Ce(IV) satellite peak at 916.8 eV decreased significantly, and the concentration of Ce(III) increased from 26.6% to 62.1%; the increased amount of Ce(III) may facilitate subsequent electron transfer. To investigate the interactions between the Pd nanoparticles and MOF host, the Pd 3d XPS spectra of Pd@Ce-bptc and Pd/C were measured (Fig. 2d). The Pd 3d<sub>5/2</sub> peak for Pd@Ce-bptc was located at 335.7 eV (calibrated against the C peak 1s = 284.8 eV). Compared with the Pd 3d<sub>5/2</sub> peak of Pd/C (335.1 eV),<sup>20</sup> that for Pd@Ce-bptc was found at a higher binding energy, indicating electron transfer from Pd to Ce in Pd@Ce-bptc.<sup>21</sup> This shift in binding energy for Pd 3d<sub>5/2</sub> is not due to issues with charge calibration as other peak positions are at the expected values after calibration.

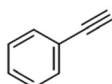
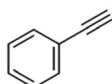
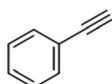
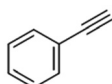
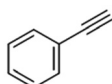
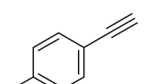
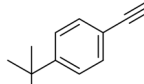
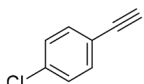
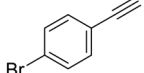
The catalytic performances of a range of Pd-based catalysts (Pd@Ce-bptc, Pd@Zr-bptc, Pd@Ce-Uio-66, Pd@Zr-Uio-66, Pd@CeO<sub>2</sub>, and Pd@ZrO<sub>2</sub>) were tested for the semi-hydrogenation of phenylacetylene (Fig. S12†). The impact of different loadings of Pd nanoparticles (0.3, 2.0, 3.7 and 5.4%) in Pd@Ce-bptc was studied. At 25 °C and under 1 bar of H<sub>2</sub> for 1 h, the conversion of phenylacetylene increased from 33% to 91% upon increasing loading of Pd nanoparticles, and the TOF decreased from 2385 to 362 h<sup>−1</sup> (Fig. 3a). To balance the TOF and conversion, Pd@Ce-bptc with 2.0 wt% of Pd was used for further tests and comparison with other catalysts.

For the reaction at 25 °C and 1 bar of H<sub>2</sub> for 2.5 h, Pd@Ce-bptc-2.0% shows a selectivity of 93% towards styrene on full conversion of phenylacetylene (Fig. 3b). Control experiments with Pd/C (Pd supported on carbon black) demonstrate >99% conversion with only 10% selectivity towards styrene (the major product is ethylbenzene), while bare Ce-bptc shows no activity (Table 1). A powdered mixture of 2% Pd/C and Ce-bptc shows a selectivity of 45% towards styrene on full conversion, demonstrating the important role of confinement of Pd nanoparticles in the pores to promote semi-hydrogenation rather than full hydrogenation. The selectivity of Pd@Ce-bptc-2.0% is higher than that of the commercial Lindlar catalyst (which shows a selectivity of 87% on full conversion), other supported Pd@MOF catalysts (Pd@Ce-Uio-66, Pd@Zr-bptc, and Pd@Zr-Uio-66) and metal oxides (Pd@CeO<sub>2</sub> and Pd@ZrO<sub>2</sub>) (Table 1). To explore its reusability, used Pd@Ce-bptc was tested for 5



**Fig. 3** Studies of catalytic performance. Reaction conditions: 5 mg of MOF catalyst, 1 mmol of phenylacetylene, 1 mmol of mesitylene, 2 mL of THF, 25 °C, 2.5 h. (a) Conversion of phenylacetylene and selectivity for styrene on Pd@Ce-bptc at different Pd loadings. (b) Conversion of phenylacetylene and selectivity for styrene on Pd@Ce-bptc-2.0% over time. (c) Recycling test for Pd@Ce-bptc. (d) Comparison of the catalytic performance of different Pd-loaded catalysts under 1 bar H<sub>2</sub>.

**Table 1** Summary of catalytic activity for semi-hydrogenation of alkynes to alkenes

| Catalyst  | Substrate   | Time (h) | Conv. (%) | Sel. of alkene (%) |
|---|---|----------|-----------|--------------------|
| Pd@Ce-bptc-2.0% powdered mixture of 2%Pd/C + Ce-bptc                                  |  | 2.5      | >99       | 93                 |
|   |   | 2.5      | >99       | 45                 |
| Pd@Zr-bptc-2.2%   |  | 2.5      | >99       | 91                 |
| Pd@Ce-UiO-66-2.0%   |   | 3        | >99       | 88                 |
| Pd@Zr-UiO-66-2.1%   |  | 6        | >99       | 85                 |
| Pd@CeO <sub>2</sub> -2.0%   |   | 2.5      | >99       | 71                 |
| Pd@ZrO <sub>2</sub> -2.1%   |  | 2.5      | >99       | 17                 |
| 2%Pd/C  |   | 2.5      | >99       | 10                 |
| Ce-bptc   |  | 2.5      | 0         | 0                  |
| Pd@Ce-bptc-2.0%   |   | 1.0      | 52        | 99                 |
| Pd@Ce-bptc-2.0%   |  | 1.0      | 55        | 93                 |
| Pd@Ce-bptc-2.0%   |   | 1.0      | 85        | 89                 |
|  |   |          |           |                    |
| Pd@Ce-bptc-2.0%   |  | 1.0      | 42        | 86                 |
| Pd@Ce-bptc-2.0%   |  | 1.0      | 20        | 90                 |

Reaction conditions: 5 mg of catalyst, 1 mmol of substrate, 1 mmol of mesitylene as internal standard, 2 mL of THF, 25 °C water bath, 1 bar H<sub>2</sub> balloon.



consecutive runs, and the conversion of phenylacetylene remained at 97%. After 5 consecutive runs, the PXRD pattern of the used catalyst did not show any obvious changes, demonstrating its high stability (Fig. 3c and Fig. S14†). In comparison, the conversion over Pd@Zr-bptc decreased from 98% to 88% after 5 runs (Fig. S15†). The improved stability of Pd@Ce-bptc compared with Pd@Zr-bptc is consistent with the XPS result, which shows stronger interaction between Pd nanoparticles and Ce-bptc (Fig. 2d and S12†).

The semi-hydrogenation of phenylacetylene-based substrates with various *para*-substitutions was tested over Pd@Ce-bptc to investigate the impact of substitution groups on the reaction (Table 1). The reaction time for all substrates was set at 1 h, and conversions for 4-methylphenylacetylene, 4-*tert*-butylphenylacetylene, 4-chlorophenylacetylene and 4-bromophenylacetylene of 55%, 85%, 42% and 20%, respectively, were observed (Fig. S16–20†). These results suggest that substrates with an electron-donating group show higher conversions compared with phenylacetylene, while substrates with an electron-withdrawing group show lower conversions. Overall, these results suggest that Pd@Ce-bptc is a highly active and stable catalyst for semi-hydrogenation at room temperature.

To investigate the host-guest interaction between the adsorbed substrate and Ce-bptc, SXPD data were collected for phenylacetylene-loaded Ce-bptc, and highly satisfactory Rietveld refinement revealed the binding domains for the substrate (Fig. 4a, S20 and Table S1†). The ethynyl group of

adsorbed phenylacetylene interacts with the bridging oxygen and carboxylate oxygen centres of the  $\{Ce_6O_6\}$  clusters to form hydrogen bonds [ $C\equiv C-H\cdots O_{bridge} = 3.46(5)$  Å,  $C\equiv C-H\cdots O_{ligand} = 3.15(8)$  Å]. These adsorbed molecules are further stabilised by parallel-displaced  $\pi\cdots\pi$  interactions between the  $C\equiv C$  bond/benzene rings of guest molecules and ligands of Ce-bptc, with inter-planar distances of 4.02(1) Å and 4.09(1) Å, respectively. Thus, the SPXRD study confirms the presence of notable host-guest binding interactions that facilitate charge transfer and thus promote hydrogenation.<sup>22,23</sup>

It has been reported that the hydrogenation of phenylacetylene to styrene and ethylbenzene may proceed *via* two different mechanisms: so-called one-pathway or two-pathway.<sup>24</sup> The one-pathway mechanism involves direct hydrogenation of the triple bond to a single bond, while the two-pathway mechanism proposes a two-step hydrogenation process involving the formation of single or multiple adsorbed species.<sup>25,26</sup> Given the high selectivity towards styrene observed for Pd@Ce-bptc, it is suggested that the reaction predominantly follows the two-pathway mechanism involving adsorbed intermediates.

To identify any radical species in this reaction, *in situ* EPR spin-trapping experiments were conducted. Considering the transient nature of many free radicals, with lifetimes significantly shorter than the acquisition time of EPR spectra, *N*-*tert*-butyl- $\alpha$ -phenylnitrone (PBN) was employed as a spin trap reagent<sup>27</sup> to identify radicals as long-lived PBN-radical

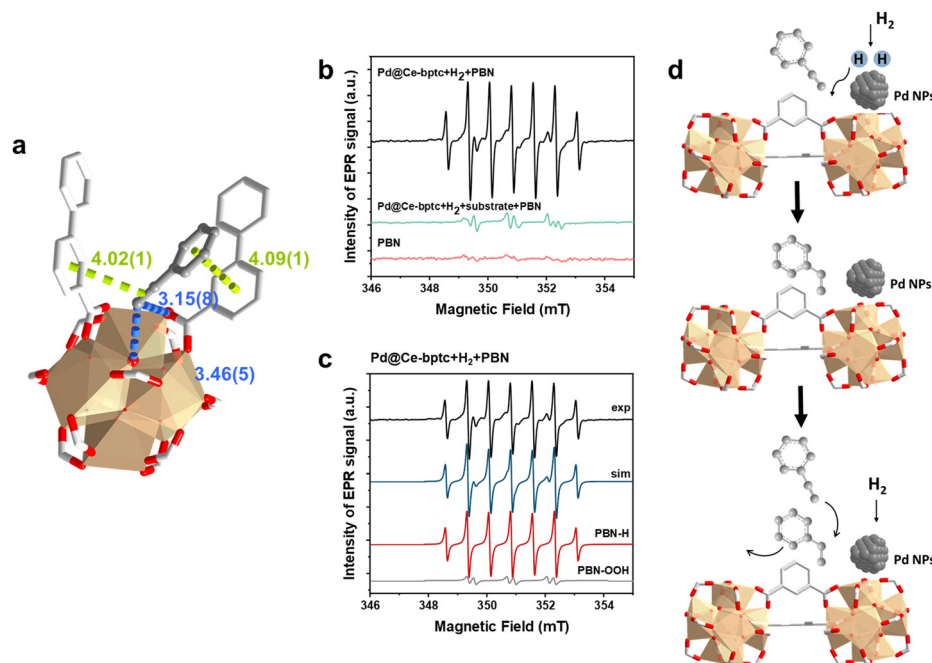


**Fig. 4** Studies of the mechanism of catalysis. (a) Views of the crystal structure of phenylacetylene-loaded Ce-bptc obtained from Rietveld refinements of SXPD data. The guest molecules are highlighted using an amplified ball-and-stick model; hydrogen atoms are omitted for clarity. Bond distances are in angstroms. (b) *In situ* X-band EPR spectra under controlled conditions using PBN as a spin trap reagent. Top to bottom: Pd@Ce-bptc + H<sub>2</sub> + THF; Pd@Ce-bptc + H<sub>2</sub> + phenylacetylene + THF; PBN (THF solution). (c) Experimental and simulated spectra of the black spectrum in (b), showing a major component, PBN-H (red, simulation), and a minor component, PBN-OOH (grey, simulation). (d) Schematic of the proposed reaction mechanism for semi-hydrogenation of phenylacetylene (NPs = nanoparticles).





adducts. When  $H_2$  and the catalyst were present in the reaction solution, an intense seven-line EPR signal with a  $g$ -factor of 2.0055 and hyperfine coupling constants  $A^N = 15.0$  G and  $A^{H_1} = A^{H_2} = 7.4$  G was detected. This signal is unequivocally attributed to the PBN-H radical,<sup>28</sup> indicating that  $H_2$  is activated directly by the confined Pd nanoparticles, leading to homolytic dissociation of the H–H bond and the generation of  $H^\bullet$  radicals (Fig. 4b, c and Table S2†). Interestingly, no PBN-H signal was observed when the substrate was added to the reaction solution, suggesting that the hydrogenation involving  $H^\bullet$  radicals and the substrate is extremely rapid, preventing  $H^\bullet$  radicals from being trapped by PBN (Fig. S22†). Thus, the EPR study confirms the reaction pathway (Fig. 4d):  $H_2$  is first activated by the Pd nanoparticles, resulting in the homolytic dissociation of the H–H bond and the release of  $H^\bullet$  radicals, which subsequently attack the  $C\equiv C$  bond of adsorbed phenylacetylene, forming the desired product, styrene, which can readily desorb from the adsorption site in competitive adsorption with phenylacetylene, thus avoiding over-hydrogenation to ethylbenzene.

## Conclusions

In summary, we report a novel cerium(IV)-based MOF, Ce-bptc, which comprises  $\{Ce_6O_4(OH)_4(CO_2)_{12}\}$  clusters that are further bridged by tetracarboxylate ligands to afford an open framework of *ftw* topology. Encapsulation of Pd nanoparticles gives a highly efficient Pd@Ce-bptc catalyst, which exhibits excellent catalytic performance for the semi-hydrogenation of phenylacetylene, achieving a selectivity of 93% towards styrene on full conversion at 25 °C and 1 bar  $H_2$ . The molecular details of host–guest interactions between the adsorbed substrate and MOF host were investigated by SXPD analysis. *In situ* EPR studies revealed the mechanism of  $H_2$  splitting and rapid hydrogenation *via*  $H^\bullet$  radicals. This study highlights the great potential of Ce-based MOFs as a catalyst support for semi-hydrogenation reactions, offering advantages in selectivity over traditional supports based upon metal oxides.

## Author contributions

XZ, WL, WH, BA, JL and ML: synthesis and characterisation of materials, catalysis testing and data analysis; ZW, FT and EJLM: collection and analysis of EPR data; MH and SJD: collection and analysis of synchrotron X-ray diffraction data; BFS: collection and analysis of XPS data; MS and SY: overall direction and supervision of the project; and XZ, MS and SY: preparation of the manuscript with contributions from all authors.

## Data availability

All relevant data are available from the corresponding authors, and/or are included in the ESI.† The crystallographic data of the structures reported in this work have been deposited in

the Cambridge Crystallographic Data Centre (CCDC) under accession numbers CCDC: 2205374 and 2205379.†

## Conflicts of interest

The authors declare no conflicts of interest.

## Acknowledgements

We thank EPSRC (EP/I011870, EP/V056409, EP/W014521/1), the University of Manchester, the National Science Foundation of China and BNLMS for funding. This project has received funding from the European Research Council (ERC) under the European Union's Horizon 2020 research and innovation programme (grant agreement No 742401, NANOCHM and PoC665632). We thank Diamond Light Source for access to Beamline I11.

## References

- 1 Y. Liu, W. Guo, X. Li, P. Jiang, N. Zhang and M. Liang, Copper single-atom-covered Pt nanoparticles for selective hydrogenation of phenylacetylene, *ACS Appl. Nano Mater.*, 2021, **5**, 5292–5300.
- 2 L. Yang, Y. Jin, X. Fang, Z. Cheng and Z. Zhou, Magnetically recyclable core–shell structured Pd-based catalysts for semihydrogenation of phenylacetylene, *Ind. Eng. Chem. Res.*, 2017, **48**, 14182–14191.
- 3 M. Crespo-Quesada, F. Cárdenas-Lizana, A.-L. Dessimoz and L. Kiwi-Minsker, Modern trends in catalyst and process design for alkyne hydrogenations, *ACS Catal.*, 2012, **8**, 1773–1786.
- 4 S. A. Nikolaev, L. N. Zhanavskina, V. V. Smirnov, V. A. Averyanov and K. L. Zhanavskina, Catalytic hydrogenation of alkyne and alkadiene impurities from alkenes. Practical and theoretical aspects, *Russ. Chem. Rev.*, 2009, **3**, 231–247.
- 5 Q. Yang, Q. Xu and H.-L. Jiang, Metal–organic frameworks meet metal nanoparticles: Synergistic effect for enhanced catalysis, *Chem. Soc. Rev.*, 2017, **46**, 4774–4808.
- 6 J. Zhang, L. Wang, Y. Shao, Y. Wang, B. C. Gates and F.-S. Xiao, A Pd@ zeolite catalyst for nitroarene hydrogenation with high product selectivity by sterically controlled adsorption in the zeolite micropores, *Angew. Chem., Int. Ed.*, 2017, **56**, 9747–9751.
- 7 H. Q. Wu, L. Huang, J. Q. Li, A. M. Zheng, Y. Tao, L. X. Yang, W. H. Yin and F. Luo, Pd@ Zn-MOF-74: Restricting a guest molecule by the open-metal site in a metal–organic framework for selective semihydrogenation, *Inorg. Chem.*, 2018, **20**, 12444–12447.
- 8 L. Chen, B. Huang, X. Qiu, X. Wang, R. Luque and Y. Li, Seed-mediated growth of MOF-encapsulated Pd@ Ag core–shell nanoparticles: Toward advanced room temperature nanocatalysts, *Chem. Sci.*, 2016, **1**, 228–233.



- 9 K. Choe, F. Zheng, H. Wang, Y. Yuan, W. Zhao, G. Xue, X. Qiu, M. Ri, X. Shi, Y. Wang, G. Li and Z. Tang, Fast and selective semihydrogenation of alkynes by palladium nanoparticles sandwiched in metal–organic frameworks, *Angew. Chem., Int. Ed.*, 2020, **9**, 3650–3657.
- 10 L. Li, W. Yang, Q. Yang, Q. Guan, J. Lu, S.-H. Yu and H.-L. Jiang, Accelerating chemo- and regioselective hydrogenation of alkynes over bimetallic nanoparticles in a metal–organic framework, *ACS Catal.*, 2020, **14**, 7753–7762.
- 11 M. Guo, Q. Meng, W. Chen, Z. Meng, M.-L. Gao, Q. Li, X. Duan and H.-L. Jiang, Dual microenvironment modulation of Pd nanoparticles in covalent organic frameworks for semihydrogenation of alkynes, *Angew. Chem., Int. Ed.*, 2023, **62**, e202305212.
- 12 J. Jacobsen, A. Ienco, R. D'Amato, F. Costantino and N. Stock, The chemistry of Ce-based metal–organic frameworks, *Dalton Trans.*, 2020, **49**, 16551–16586.
- 13 M. Lammert, M. T. Wharmby, S. Smolders, B. Bueken, A. Lieb, K. A. Lomachenko, D. D. Vos and N. Stock, Cerium-based metal organic frameworks with UiO-66 architecture: synthesis, properties and redox catalytic activity, *Chem. Commun.*, 2015, **51**, 12578–12581.
- 14 X. He, B. G. Looker, K. T. Dinh, A. W. Stubbs, T. Chen, R. J. Meyer, P. Serna, Y. Román-Leshkov, K. M. Lancaster and M. Dincă, Cerium(IV) enhances the catalytic oxidation activity of single-site Cu active sites in MOFs, *ACS Catal.*, 2020, **14**, 7820–7825.
- 15 H. Wang, X. Dong, J. Lin, S. J. Teat, S. Jensen, J. Cure, E. V. Alexandrov, Q. Xia, K. Tan, Q. Wang, D. H. Olson, D. M. Proserpio, Y. J. Chabal, T. Thonhauser, J. Sun, Y. Han and J. Li, Topologically guided tuning of Zr-MOF pore structures for highly selective separation of C6 alkane isomers, *Nat. Commun.*, 2018, **9**, 1745.
- 16 J. Li, G. L. Smith, Y. Chen, Y. Ma, M. Kippax-Jones, M. Fan, W. Lu, M. D. Frogley, G. Cinque, S. J. Day, S. P. Thompson, Y. Cheng, L. L. Daemen, A. J. Ramirez-Cuesta, M. Schröder and S. Yang, Structural and dynamic analysis of sulphur dioxide adsorption in a series of zirconium-based metal–organic frameworks, *Angew. Chem., Int. Ed.*, 2022, **61**, e202207259.
- 17 A. Aijaz, A. Karkamkar, Y. J. Choi, N. Tsumori, E. Rönnebro, T. Autrey, H. Shioyama and Q. Xu, Immobilizing highly catalytically active Pt nanoparticles inside the pores of metal–organic framework: A double solvents approach, *J. Am. Chem. Soc.*, 2012, **34**, 13926–13929.
- 18 Y. A. Teterin, A. Y. Teterin, A. M. Lebedev and I. O. Utkin, The XPS spectra of cerium compounds containing oxygen, *J. Electron Spectrosc. Relat. Phenom.*, 1998, **88**, 275–279.
- 19 H. Chen, C. Liu, W. Guo, Z. Wang, Y. Shi, Y. Yu and L. Wu, Functionalized UiO-66 (Ce) for photocatalytic organic transformation: The role of active sites modulated by ligand functionalization, *Catal. Sci. Technol.*, 2022, **6**, 1812–1823.
- 20 C. Wang, Y. Jia, Z. Zhang, G. Zhao, Y. Liu and Y. Lu, Role of PdCx species in Pd@PdCx/AlOOH/Al-fiber catalyst for the CO oxidative coupling to dimethyl oxalate, *Appl. Surf. Sci.*, 2019, **478**, 840–845.
- 21 L. Li, Y. Li, L. Jiao, X. Liu, Z. Ma, Y.-J. Zeng, X. Zheng and H.-L. Jiang, Light-induced selective hydrogenation over PdAg nanocages in hollow MOF microenvironment, *J. Am. Chem. Soc.*, 2022, **37**, 17075–17085.
- 22 Y. Chen, W. Lu, M. Schröder and S. Yang, Analysis and refinement of host–guest interactions in metal–organic frameworks, *Acc. Chem. Res.*, 2023, **19**, 2569–2581.
- 23 J. Wang, Y. Cao, Q.-W. Meng, Y. Wang, H. Shi, B. Feng, Y. Huang, Q. Sun and L. He, Catalysis of synergistic reactions by host–guest assemblies: reductive carbonylation of nitrobenzenes, *JACS Au*, 2023, **8**, 2166–2173.
- 24 B. A. Willhite, M. J. McCready and A. Varma, Kinetics of phenylacetylene hydrogenation over Pt/ $\gamma$ -Al<sub>2</sub>O<sub>3</sub> catalyst, *Ind. Eng. Chem. Res.*, 2002, **14**, 3345–3350.
- 25 C. Zhang, L. Wu, R. Ye, G. Feng and R. Zhang, Promoter effect on Ni/SiO<sub>2</sub> catalysts for acetylene semi-hydrogenation to ethylene, *Catal. Lett.*, 2024, **154**, 3619–3627.
- 26 D. Wang, R. Ye, C. Zhang, C. Jin, Z. Lu, M. Shakouri, B. Han, T. Wang, Y. Zhang, R. Zhang, Y. Hu, J. Zhou and G. Feng, Robust Ni<sub>x</sub>Sn/ZSM-12 catalysts with zeolite as the support and Sn as the promoter for acetylene semi-hydrogenation, *Energy Fuels*, 2023, **37**, 13305–13318.
- 27 Y. Gorbanev, N. Stehling, D. O'Connell and V. Chechik, Reactions of nitroxide radicals in aqueous solutions exposed to non-thermal plasma: Limitations of spin trapping of the plasma induced species, *Plasma Sources Sci. Technol.*, 2016, **25**, 055017.
- 28 Y. Gorbanev, C. C. W. Verlackt, S. Tinck, E. Tüenter, K. Foubert, P. Cos and A. Bogaerts, Combining experimental and modelling approaches to study the sources of reactive species induced in water by the COST RF plasma jet, *Phys. Chem. Chem. Phys.*, 2018, **20**, 2797–2808.

